Effects of N_2/O_2 flow rate on the surface properties and biocompatibility of nano-structured TiO_xN_y thin films prepared by high vacuum magnetron sputtering*

Sehrish Saleem[a)b)], R. Ahmad[a)†], Uzma Ikhlaq[a)], R. Ayub[c)], Jin Wei Hong[b)], Xu Rui Zhen[b)], Li Peng Hui[b)], Khizra Abbas[a)], and Paul K. Chu[b)]

[a)] *Department of Physics, Government College University, Lahore* 54000, *Pakistan*
[b)] *Department of Physics and Materials Science, City University of Hong Kong, Kowloon, Hong Kong, China*
[c)] *Centre for Advanced Studies in Physics (CASP), Government College University, Lahore* 54000, *Pakistan*

(Received 8 September 2014; revised manuscript received 19 February 2015; published online 29 May 2015)

NiTi shape memory alloys (SMA) have many biomedical applications due to their excellent mechanical and biocompatible properties. However, nickel in the alloy may cause allergic and toxic reactions, which limit some applications. In this work, titanium oxynitride films were deposited on NiTi samples by high vacuum magnetron sputtering for various nitrogen and oxygen gas flow rates. The x-ray diffraction (XRD) and x-ray photoelectron spectroscopy (XPS) results reveal the presence of different phases in the titanium oxynitride thin films. Energy dispersive spectroscopy (EDS) elemental mapping of samples after immersion in simulated body fluids (SBF) shows that Ni is depleted from the surface and cell cultures corroborate the enhanced biocompatibility in vitro.

Keywords: titanium oxynitride films, magnetron sputtering, biocompatibility

PACS: 52.40.Hf, 81.15.Cd, 87.85.jj **DOI:** 10.1088/1674-1056/24/7/075202

1. Introduction

Shape memory effects and superelasticity are the two main properties of NiTi shape memory alloys (SMA) which make them important materials for different applications.[1–3] Due to their high corrosion resistance, good biocompatibility, and excellent mechanical properties, NiTi alloys have been widely used in medical fields, such as orthodontic arc wires, cardiovascular stents, and orthopedic devices.[4–8] However, more widespread use of NiTi is hampered by the large contents of Ni which may cause cellular inflammation as well as toxic and allergic reaction. It may also be carcinogenic in case of prolonged exposure. Hence, it is important to prevent or at least minimize Ni ion release from NiTi SMA implants. Biocompatibility of NiTi alloys can be improved by minimizing the release of Ni. For this purpose, surface modification of NiTi alloys are carried out by different techniques such as sol-gel method, plasma immersion ion implantation, plasma spray, and plasma deposition.[9–12] The key advantage of plasma surface modification is its ability to improve only selective surface properties, whereas the bulk properties remain the same.[11]

Several research groups have made great effort to enhance the bioactivity of NiTi alloy. Liu *et al.*[9] mentioned that the formation of TiO_2 layer on NiTi substrate, improved the corrosion and blood compatibility. Sun *et al.*[10] concluded that (Ti, O, N)/Ti composite coating was best for medical applications because it improves the biocompatibility, wear resistance, and mechanical properties of NiTi alloy. More recently, Hossary *et al.*[13] found that plasma nitriding formed the TiN layer, which not only enhanced the corrosion resistance, but also effectively prevented the Ni release from the NiTi surface.

From the literature, it is clear that biocompatibility of NiTi alloys are mostly studied after formation of oxide or nitride layer on NiTi surface. Recently, metallic oxynitrides have attracted much scientific interest owing to their diverse properties.[14–16] Therefore, in the present study, we investigate and compare the effects of the gas flow rate on the properties of titanium oxynitride thin films deposited by reactive magnetron sputtering. The surface chemistry and morphology are evaluated and discussed together with the biological results.

2. Experimental details

Ni (50.8 at.%) Ti alloys (SE508) samples purchased from Nitinol Device Company, Fremont, USA were used as substrate in this experiment. The samples were mechanically grounded with 200, 400, 600, 800, 1000, and 1200 grit SiC paper, cleaned with ethanol, acetone, and distilled water sequentially for 10 min in an ultrasonic bath, and air dried. A round-shaped Ti (99.99%) purity with 0.25 inch thickness and 2 inch diameter are used as target for sputtering. Deposition was performed in the ultra-high vacuum PVD system (mag-

*Project supported by the Higher Education Commission, Hong Kong Research Grants Council (RGC) General Research Funds (GRF), China (Grant No. 112212) and the City University of Hong Kong Applied Research Grant (ARG), China (Grant No. 9667066).

†Corresponding author. E-mail: ahriaz@gcu.edu.pk

© 2015 Chinese Physical Society and IOP Publishing Ltd

netron system) in the Plasma Laboratory at City University of Hong Kong. The base vacuum was below 1.2×10^{-5} Torr and the substrate temperature during deposition was 400 °C. High-purity argon was fed into the chamber to generate the plasma generation and the substrate was first etched in an Ar flow rate of 10 sccm for 20 min at a DC power of 30 W. Afterwards, deposition proceeded for 1 h in an Ar/N_2+O_2 environment. The samples were rotated at 4 rpm and positioned at a distance of 23 mm from the target. Oxygen and nitrogen were used as reactive gases to form titanium oxynitrides along with argon as sputtering gas. The temperature (400 °C), power (400 W), and deposition time (1 hour) were kept the same, while the nitrogen to oxygen flow rate ratio was changed (1:3, 3:1, 1:1) and the Ar gas flow was constant at 5 sccm.

XRD was employed to examine the change in the preferred orientation on the X'Pert Pro diffractometer using Cu Kα (1.541 Å) radiation at 40 kV and 30 mA. The chemical composition of the outermost layer of the films were determined by x-ray photoelectron spectroscopy (XPS) (PHI Model 5802) performed at a base pressure of 10^{-8} Torr using MgK$_\alpha$ x-ray (1253.6 eV). A Gaussian peak fitting model was adopted to deconvolute the spectra using XPSPEAK41 software. Atomic force microscopy (AFM, Park Scientific Instruments) was used to determine the surface topography and roughness of the sample surface before and after deposition. Scanning electron microscopy (SEM, JEOL JSM-820) and energy-dispersive x-ray spectrometry (EDS) were utilized to examine and analyze the surface morphology and chemical composition of the specimens.

The biological experiments were conducted with MC3T3-E1 pre-osteoblasts. The cells were cultured in a high-glucose Dulbecco's modified eagle medium (DMEM) supplemented with 10% fetal bovine serum (FBS) in 75 cm^2 tissue culture flakes and were incubated in a humidified atmosphere of 5% CO_2 at 37 °C. 50000 cells in a volume 1 mL were seeded on each sample on 12-well plates for cell morphology observation and proliferation assay. After culturing for 24 h, the cells were rinsed with PBS and fixed with 4% paraformaldehyde in a humidified atmosphere of 5% CO_2 at 37 °C for 20 min. After fixing, the cells were stained with FITC-Phalloidin and 4′, 6-diamidino-2-phenylindole XRD patterns (DAPI) sequentially and then were observed by fluorescence microscopy.

3. Results and discussion

The XRD patterns are depicted in Fig. 1. It is clear that untreated NiTi sample consists of three peaks at 2θ positions of 42.56°, 61.80°, and 77.9° corresponding to (110), (200), and (211) phases for cubic structure, respectively. In the deposited samples, TiO, TiN, Ti_2N, and TiO_2 phases are observed. The existence of these new phases in deposited samples confirms the formation of titanium oxynitride film on the NiTi substrate. Since TiO or TiN has the same crystallographic structure (cubic) with very close lattice parameters as calculated for (200) and (111) phases, (i.e., $\alpha_{TiN} = 0.427$ nm and $\alpha_{TiO} = 0.429$ nm), XRD is not the suitable technique to distinguish these two structures.[17] The occurrence of TiO_2 at angels 36.7° and 54.4° having planes (211) and (202), respectively, indicates the anatase phase, whereas planes corresponding to (103) and (213) at angels 36.7° and 61.6°, respectively, are rutile. Presence of these phases is useful to improve the bioactivity as reported by Shu *et al.*,[18] and is therefore favorable for apatite growth. Liu *et al.*[9] also observed that TiO_2 layer formed on NiTi substrate consists of anatase and rutile phases, enhancing the biocompatibility of NiTi alloy. Moreover, with an increase in oxygen concentration, the intensity of R-TiO_2 (202) also increases. This increase in intensity may be attributed to more oxygen incorporation at higher concentration of oxygen because the probability of ionized oxygen is larger as compared to that of nitrogen.

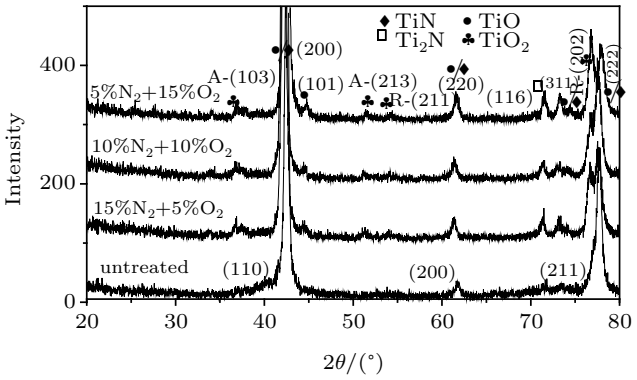


Fig. 1. XRD patterns of TiO_xN_y films deposited at different oxygen flow rates.

The evolution of the crystallite size of (200) can be estimated using Scherer's equation[19]

$$l_c = \frac{K\lambda}{\mathrm{FWHM}\cos\theta},$$

where K is a constant that depends on cell geometry (shape factor) and its value varies between 0.9–1, λ is the x-ray wavelength and is equal to 1.54 Å, the FWHM is the full width at half maxima of particular diffraction peak, and θ is Bragg's angle of the diffraction peak.

The results are 112, 21, and 74 nm for oxygen flow rates of 5, 10, and 15 sccm, respectively. The minimum value of crystallite (i.e., 21 nm) is observed at the same flow rate of nitrogen and oxygen. This variation trend of crystallite size with increasing oxygen concentration may be due to variation in oxygen incorporation.

The XPS survey scan spectra are acquired over a binding energy range from 0 to 1400 eV with an energy step of $\Delta E = 0.8$ eV (Fig. 2). The peaks are assigned to Ti, N, O, and C (surface contamination). The peaks within range from 1230 eV to 976 eV correspond to the Auger peaks of Ti LMM

OKLL and CKLL.[20] The main component of the C 1s peak at 284.93 eV corresponds to the C–C bonding. This carbon is detected due to the surface contamination from the atmosphere. No nickel peak is observed due to the titanium oxynitride surface layer which forms a barrier against Ni out-diffusion from the substrate to minimize allergic and toxic effects.[21] As the presence of oxygen in TiN coatings can promote the formation of bone-like materials *in vivo*.[22] In fact, a titanium oxynitride film on the surface is favorable to calcium phosphate nucleation due to the presence of mixed-valence states of the surface Ti atoms and localization of negative charges on the oxidized surface. The high-resolution spectra from 450 eV to 475 eV for Ti 2p, 392 eV to 408 eV for N 1s, and 525 eV to 542 eV for O 1s for samples deposited at different p (O_2)/p (N_2) flow rates are presented in Figs. 3–5. The core level spectra of the films deposited at different flow rates can be convoluted to identify various compounds/phases that have been formed on the surface of composite thin films such as nitrides, oxides, and oxynitrides in the film as given in Figs. 3–5. As shown in Fig. 3, the deconvoluted peaks of Ti 2p into Ti $2p_{3/2}$ and Ti $2p_{1/2}$ found at 459.15 eV and 458.9 eV, respectively, were identified as Ti^{4+} in TiO_2.[23] As shown in Fig. 4, the O 1s spectrum shows a shoulder peak on the high binding energy side and it can be deconvoluted into two peaks at 533.30 eV and 532.23 eV which are assigned to TiO*x*N*y* with the hydroxyl (O–H) and (C–O–C) groups.[20,24] The N-1s spectrum in Fig. 5 shows Ti–O at binding energies of 396.2 eV, Ti–N–O at 397.4 eV,[17,25] whereas the peaks at 400.3 and 402.20 eV are due to N–O bonds.[26,27] Hence, the TiO*x*N*y* films contain a mixture of Ti–N–O, Ti–N, and Ti–O chemical states and the chemical composition can be calculated using the integrated area of the Ti-2p, O-1s, and N-1s peaks.[28]

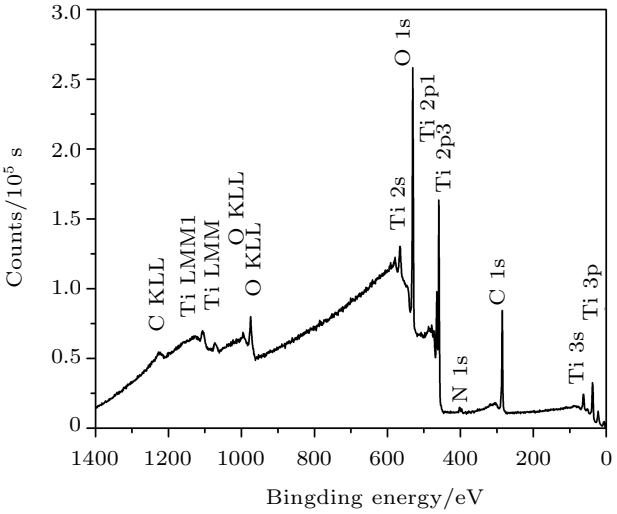


Fig. 2. XPS spectrum showing TiO_xN_y film growth.

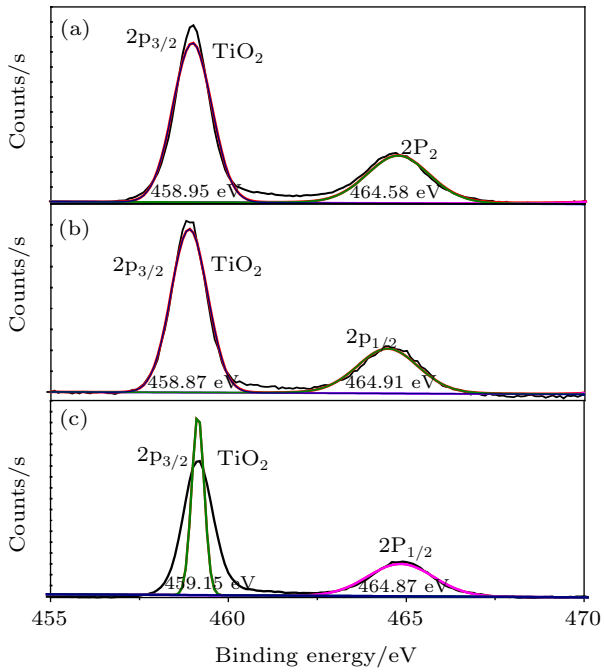


Fig. 3. (color online) High-resolution XPS spectra of Ti2p obtained from TiO_xN_y films prepared at different oxygen flow rates: (a) 15 sccm, (b) 10 sccm, and (c) 5 sccm.

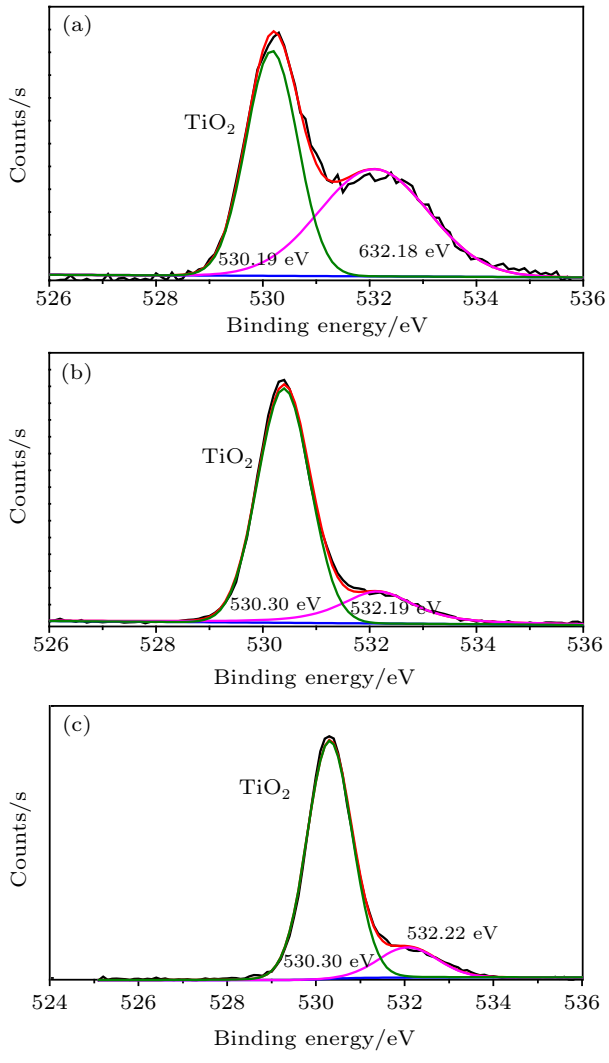


Fig. 4. (color online) High-resolution XPS spectra of O 1s obtained from TiO_xN_y films prepared at different oxygen flow rates: (a) 15 sccm, (b) 10 sccm, and (c) 5 sccm.

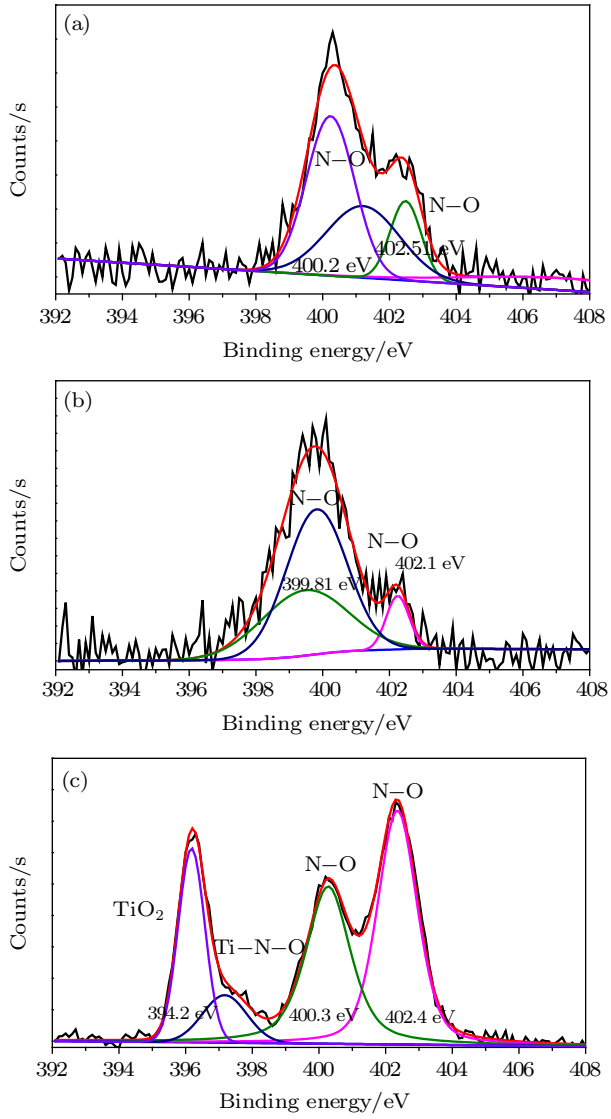


Fig. 5. (color online) High-resolution XPS spectra of N 1s obtained from TiO_xN_y films prepared at different oxygen flow rates: (a) 15 sccm, (b) 10 sccm, and (c) 5 sccm.

The surface morphology before and after titanium oxynitride deposition on NiTi alloy was studied by AFM and given in Fig. 6. Figure 6(a) depicts that the surface of untreated NiTi alloy is quite smooth and almost free of particles. However, the surface of treated specimen consists of uniformly-distributed, large dome-shaped islands (spiky cones) which become smooth and then again enhance with increasing oxygen flow rates (Figs. 4(b)–4(d)). The occurrence of large dome-shaped islands confirms the formation of titanium oxynitride film on substrate surface. The surface roughness parameters, namely, R_q (root mean square (RMS)), R_a (average roughness), and R_z (ten-point mean height), before and after deposition are listed in Table 1. The 3D micrographs indicate that the roughness of treated specimens is higher as compared to the untreated specimen. Moreover, roughness increases with increase in oxygen concentration. It is quoted in the literature that the rough surface is more favorable, to enhance the biocompatibility of material, as compared to smooth surface.[29] Wirth *et al.*[30] specified that a rough surface was more beneficial to stimulate the cell proliferation. In addition, it does not affect the osteoblasts morphology. The increase in biocompatibility with roughness may be due to rough surface providing more surface area for initial cell attachment. The increase in available surface area can enhance the bioactivity, and thus the rate of bone formation also improves. The increase in surface roughness of the NiTi alloy after titanium oxynitride formation is attributed to the growth mechanism which is influenced by both the sputtering and deposition effects.[31]

Table 1. Roughness values of untreated and deposited films.

(O_2/N_2)/sccm	R_q/nm	R_a/nm	R_z/nm
untreated	7.98	6.46	3.96
5:15	8.11	6.44	9.65
10:10	8.95	7.21	17.9
15:5	19.2	15.5	17.8

EDS results after immersing in simulated body fluid (SBF) with a pH of 7.42 at 37 ± 0.5 °C for 3 days are shown in Table 2. The SBF which mimics human body fluids, has the following composition: 7.996 g/L of NaCl, 0.35 g/L of $NaHCO_3$, 0.224 g/L of KCl, 0.228 g/L of $K_2HPO_4.3H_2O$, 0.305 g/L of $MgCl_2.6H_2O$, 0.278 g/L of $CaCl_2$, 0.071 g/L of Na_2SO_4, as well as 6.057 g/L $(CH_2OH)_3CNH_2$.[32] The results show the distribution of Ti, Ni, Ca, P, N and O, confirming the presence of the deposited film. The concentration of nitrogen and oxygen is significant as compared to that of other elements. Although the amounts of Ca and P are insignificant, a large amount of surface nitrogen and oxygen acts as barrier against nickel release. Sufficient blocking of Ni release from the NiTi-SMA is imperative to biomedical implants because even a small amount of Ni (e.g., 0.5 ppm) has been reported to induce allergic reactions[33] and strong adverse reactions of osteoblasts have been observed *in vitro*.[34]

Table 2. Elemental concentrations of the films.

	Relative concentrations/at.%					
	N	O	Ca	P	Ti	Ni
untreated	–	–	–	–	51.40	48.60
5 sccm	93.03	7.21	−0.10	0.13	−0.15	−0.12
10 sccm	88	13	−0.01	0.01	−0.75	−0.66
15 sccm	61.29	27.91	0.06	−0.05	5.66	5.01

In order to study the biological acceptability, mouse MC3T3-E1 pre-osteoblasts are cultured. Figure 7 displays the fluorescent microscopy images of the cells after 3 days. The cells can clearly attach and proliferate on the samples and no obvious cytotoxic effects can be observed from the deposited samples. The MC3T3-E1 cells on the samples prepared at 5 and 15 sccm oxygen flow rates have higher activity than those treated at 10 sccm. The rectangular and elongated morphologies of the cells in Figs. 7(a) and 7(c) reveal the tendency to occupy a larger area compared to the film deposited at the same

flow rate of oxygen and nitrogen in Fig. 7(b) which shows a triangular morphology. Titanium oxynitride has formed a dense layer on the NiTi surface, which acts as barrier and stops the Ni release from the substrate. The cell reaction is governed by the coating instead of the substrate, thus providing the opportunity for accelerated tissue repair and regeneration.[35]

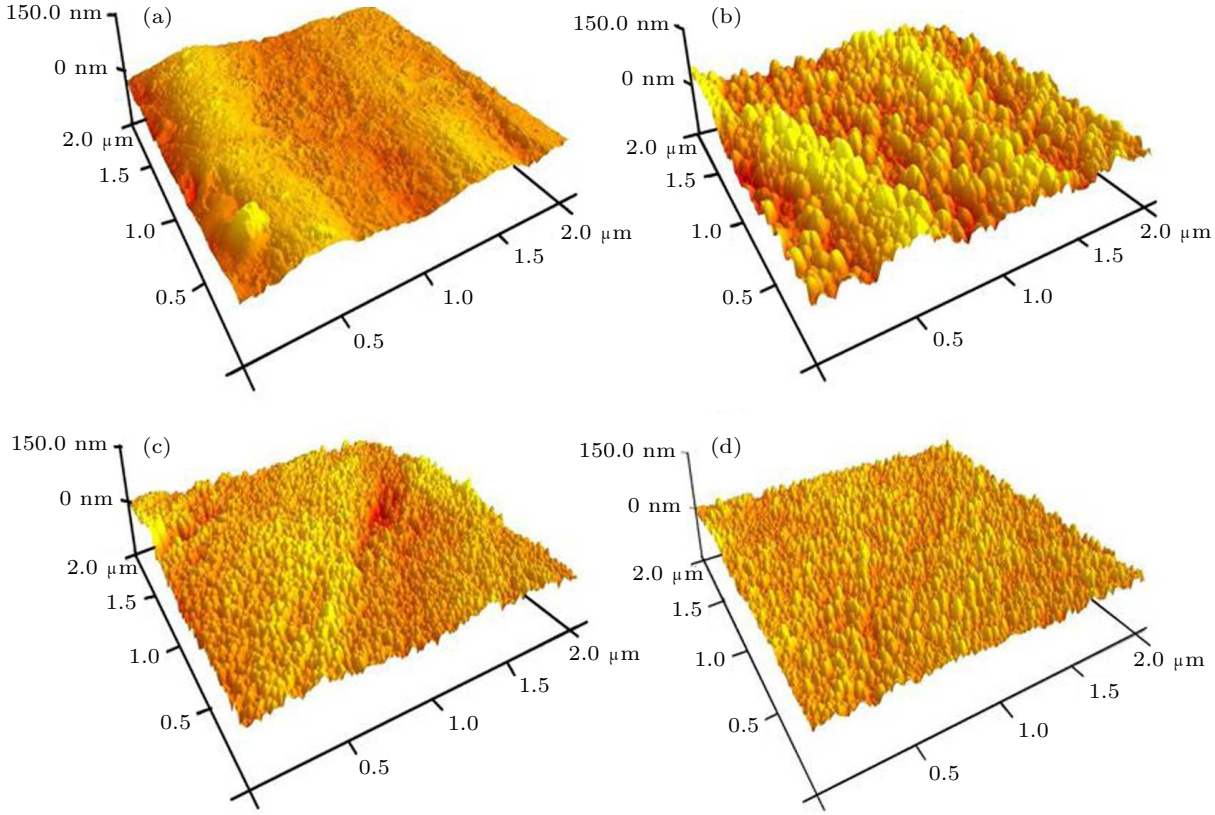


Fig. 6. (color online) AFM surface morphology: (a) untreated, (b) 5 sccm, (c) 10 sccm, and (d) 15 sccm oxygen flow rate.

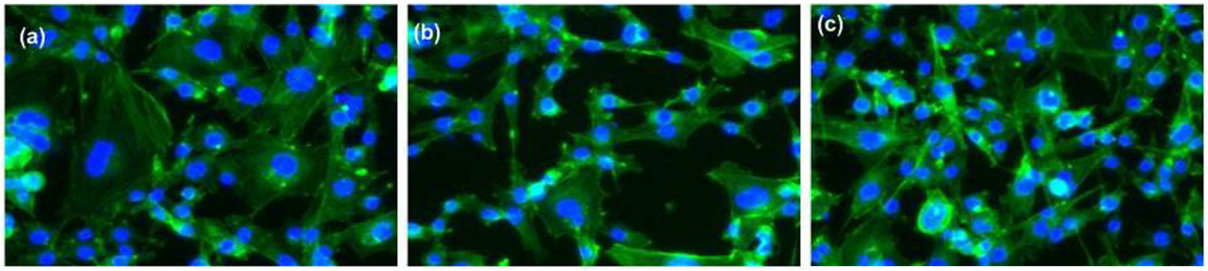


Fig. 7. (color online) Fluorescence microscopy images after culturing for 3 days: (a) 5 sccm, (b) 10 sccm, and (c) 15 sccm oxygen flow rate.

4. Conclusion

Titanium oxynitride films are deposited on NiTi by DC reactive magnetron sputtering using different flow rate ratios of nitrogen to oxygen and the effects of the flow rates on the surface and biological properties are investigated. The analysis of XRD and XPS confirm the presence of titanium oxynitride film on the NiTi substrate. The surface morphology results indicate that after titanium oxynitride deposition the roughness of NiTi surface increases, which promotes the cell adhesion proliferation. EDS results show insignificant amount of calcium and phosphorus, but the oxynitride film acts as a barrier against out-diffusion of nickel. Cell cultures indicate that the NiTi with surface titanium oxynitride fosters proliferation and shows no obvious cytotoxicity.

Acknowledgments

The authors are grateful to Mr. Wang Chen-Xi and other members of the Plasma Laboratory of City University of Hong Kong for experimental assistance and S. Lau for experimental assistance for SEM and AFM.

References

[1] Falvo A, Furgiuele F M and Maletta C 2005 *Mater. Sci. Eng. A* **412** 235
[2] Tang C, Huang W M, Wang C C and Purnawali H 2012 *Smart Mater. Struct.* **21** 085022
[3] Soul H and Yawny A 2013 *Smart Mater. Struct.* **22** 035017
[4] Fernandes D J, Peres R V, Mendes A M and Elias C N 2011 *ISRN Dent.* **2011** 132408
[5] Petrini L and Migliavacca F 2011 *Journal of Metallurgy* **2011** 501483
[6] Camargo E N, Lobo A O, Silva M M, Ueda M, Garcia E E, Pichon L, Reuther H and Otubo J 2011 *J. Mat. Eng. Perf.* **20** 798
[7] Jin S, Zhang Y, Wang Q, Zhang D and Zhang S 2013 *Colloids Surf. B: Biointerfaces* **101** 343
[8] Liu X M, Wu S L, Chan Y L, Chu P K, Chung C Y, Chu C L, Yeung K W K, Lu W W Cheung K M C and Luk K D K 2007 *J. Biomed. Mater. Res. A* **82A** 469
[9] Liu J X, Yang D Z, Shi F and Cai Y J 2003 *Thin Solid Film.* **429** 225
[10] Sun T, Wang L P, Wang M, Tong H W and Lu W W 2012 *Mater. Sci. Eng. C* **32** 1469
[11] Lu T, Qiao Y Q and Liu X Y 2012 *Interface Focus* **2** 325
[12] Gupta R and Kumar A 2008 *Biomed. Mater.* **3** 034005
[13] El-Hossary F M, Khalil S M, Kassem M A W, El Lateef M A and Lotfy K 2014 *Journal of Basic and Applied Physics* **3** 54
[14] Scopel W L, Fantini M C A, Alayo M I and Pereyra I 2002 *Thin Solid Film.* **413** 59
[15] Richthofen A V, Domnick R, Cremer R and Neuschutz D 1998 *Thin Solid Film.* **317** 282
[16] Futsuhara M, Yoshioka K and Takai O 1998 *Thin Solid Film.* **317** 322
[17] Chappe J M, Martin N, Terwagne G, Lintymer J, Gavoille J and Takadoum J 2003 *Thin Solid Film.* **440** 66
[18] Shu Q W, Zhong X X, Wu J D, Sun J and Ostrikov K 2009 *Plasma Sci. Technol.* **11** 477
[19] Cullity B D and Stock S R 2001 Elements of x-ray Diffraction, 3rd edn., (New-Jersey: Prentice Hall) p. 388
[20] Cheng Y and Zheng Y F 2007 *Surf. Coat. Technol.* **201** 6869
[21] Moritz N, Jokinen M, Peltola T, Areva S and Yli-Urpo A 2003 *J. Biomed. Mater. Res. A* **65** 9
[22] Piscanec S, Ciacchi L C, Vesselli E, Comelli G, Sbaizero O, Meriani S and Vita A D 2004 *Acta Mater.* **52** 1237
[23] Bertoti I, Mohai M, Sullivan J L and Saicd S O 1995 *Appl. Surf.* **84** 357
[24] Kerber S J, Bruckner J J, Woziak K, Seal S, Hardcastle S and Barr T L 1996 *J. Vac. Sci. Technol. A* **14** 1314
[25] Shinn C H, Bugli G and Mariadassou G D 1991 *J. Solid State Chem.* **95** 145
[26] Gammon W J, Kraft O, Reilly A C and Holloway B C 2003 *Carbon* **41** 1917
[27] Dementjev A P, de Graaf A, de Sanden M C M V, Maslakov K I, Naumkin A V and Serov A A 2000 *Diamond and Related Materials* **9** 1904
[28] Cuong N D, Kim D J, Kang B D and Yoon S G 2006 *J. Electrochem. Soc.* **153** G856
[29] Huang H H, Ho C T, Lee T H, Lee T L, Liao K K and Chen F L 2004 *Biomol. Eng.* **21** 93
[30] Wirth C, Grosgogeat B, Lagneau C, Jaffrezic-Renault N and Ponsonnet L 2008 *Mater. Sci. Eng. C* **28** 990
[31] Huang C F, Cheng H C, Liu C M, Chen C C and Ou K L 2009 *J. Alloy. Compound.* **476** 683
[32] Kokubo T, Kushitani h, Sakka S, Kitsugi T and Yamamuro T 1990 *J. Biomed. Mater. Res.* **24** 721
[33] Menne T 1994 *Sci. Total Env.* **148** 275
[34] Hallab N J, Vermes C, Messina C, Roebuck K A, Glant T T and Jacobs J J 2002 *J. Biomed. Mater. Res.* **60** 420
[35] Horowitz M C 1998 *J. Clin. Dens.* **1** 187